Atmospheric Environment 115 (2015) 101–109

Contents lists available at ScienceDirect

Atmospheric Environment

journal homepage: www.elsevier.com/locate/atmosenv

# Estimation of point source fugitive emission rates from a single sensor time series: A conditionally-sampled Gaussian plume reconstruction

Tierney A. Foster-Wittig [a, *], Eben D. Thoma [b], John D. Albertson [a]

[a] Duke University, Department of Civil and Environmental Engineering, Durham, NC 27708, USA
[b] U.S. EPA, Office of Research and Development, National Risk Management Research Laboratory, 109 TW Alexander Drive, E343-02, RTP, NC 27711, USA

## HIGHLIGHTS

- Advancing a standardized mobile measurement method for fugitive point sources.
- 106 controlled release and 7 field study observations using a single sensor.
- Lateral Gaussian plume reconstructed from the fluctuating wind direction.
- Crosswind plume spread is estimated with both a modeled and reconstructed method.
- Results yield percent errors of −5 and −2% with standard deviation of 29 and 25%.

## ARTICLE INFO

*Article history:*
Received 2 December 2014
Received in revised form
18 April 2015
Accepted 20 May 2015
Available online 21 May 2015

*Keywords:*
Gaussian dispersion
Oil
Natural gas
Methane
Fugitive emissions
OTM 33A

## ABSTRACT

Emerging mobile fugitive emissions detection and measurement approaches require robust inverse source algorithms to be effective. Two Gaussian plume inverse approaches are described for estimating emission rates from ground-level point sources observed from remote vantage points. The techniques were tested using data from 41 controlled methane release experiments (14 studies) and further investigated using 7 field studies executed downwind of oil and gas well pads in Wyoming. Analyzed measurements were acquired from stationary observation locations 18–106 m downwind of the emission sources. From the fluctuating wind direction, the lateral plume geometry is reconstructed using a derived relationship between the wind direction and crosswind plume position. The crosswind plume spread is determined with both modeled and reconstructed Gaussian plume approaches and estimates of source emission rates are found through inversion. The source emission rates were compared to a simple point source Gaussian emission estimation approach that is part of Draft EPA Method OTM 33A. Compared to the known release rates, the modeled, reconstructed, and point source Gaussian controlled release results yield average percent errors of −5%, -2%, and 6% with standard deviations of 29%, 25%, and 37%, respectively. Compared to each other, the three methods agree within 30% for 78% of all 48 observations (41 CR and 7 Wyoming).



## 1. Introduction

Advances in onshore oil and natural gas (ONG) extraction technologies have led to significant increases in energy production over the last decade. Combining ONG production, it is estimated that there are over one million active wells in the U.S. (U.S. EIA, 2012a, U.S. EIA, 2012b) with half of the new oil wells drilled co-producing natural gas (U.S. EIA, 2013). The quantity and complexity of the potential air emission sources in the upstream and midstream ONG sectors make assessment of methane ($CH_4$) emissions a difficult challenge (Brantley et al., 2015; Brandt et al., 2014). Fugitive point sources, unintentional leaks of gas to the atmosphere, are one type of emission encountered in ONG production that can be positively impacted through development of cost effective leak detection approaches (U.S. EPA, 2014a; EDF, 2015; DOE ARPA-E, 2014; Carbon Limits (CL), 2013). This paper helps advance fugitive emission assessment concepts by investigating two calculation approaches for remote leak detection and monitoring applications.

* Corresponding author.
*E-mail addresses:* tf29@duke.edu (T.A. Foster-Wittig), thoma.eben@epa.gov (E.D. Thoma), john.albertson@duke.edu (J.D. Albertson).

http://dx.doi.org/10.1016/j.atmosenv.2015.05.042
1352-2310/

Fugitive point source and other types of emissions from upstream ONG production operations have been investigated in several on-site measurement studies that used various combinations of methods including EPA method 21, infrared cameras, leak bagging, and high flow sampling to locate and assess emissions (U.S. EPA, 1995, 2010; ERG, 2011; Allen et al., 2013, 2014). Although capable of high accuracy and completeness, direct on-site measurements can be time consuming and potential issues with use of commercially available high flow sampling technologies for upstream applications were recently noted (Howard et al., 2015; Brantley et al., 2015). Fugitive emissions can also originate from underground pipelines in the natural gas distribution sector where direct measurement approaches have recently been demonstrated (Lamb et al., 2015).

As a way to complement direct-on-site measurements, a growing number of groups are investigating ground-based mobile monitoring for remote detection and assessment of emissions from upstream ONG production operations. The use of instrumented vehicles typically combines the discovery of unknown sources detected along the driving route with some form of emission rate assessment that may be based on the release of a tracer gas (Allen et al., 2013; Lamb et al., 2015) or tracerless forms including both mobile flux planes (Rella et al., 2015) and inverse estimation approaches (Brantley et al., 2014). Draft EPA method OTM 33A (U.S. EPA, 2014b) combines mobile monitoring to identify emissions with a stationary observation, executed downwind of the source, that produces time-aligned wind field and concentration data useful for inverse source emission rate estimates. In addition to the ability to detect sources such as pipeline leaks, mobile approaches that do not require site access may offer implementation advantages over direct on-site measurements for some inspection applications. Remote measurements, however, may not have the same accuracy objectives as direct measurements and they produce an integrated pictures of emissions without the component-level resolution. Remote measurements, especially tracerless forms, rely on both favorable meteorological conditions for wind transport of the plume to the observing location and generally open areas to be useful (U.S. EPA, 2014a).

The emitted plume from a fugitive point source travels in the direction of the mean wind and disperses vertically and horizontally due to the intermittent mixing of turbulent eddies. A fully mobile measurement provides concentration as a function of lateral position as the sensor drives through the plume in the crosswind direction. A stationary observation can use variations in wind direction to inform plume geometry and source emissions by allowing the meandering plume to sweep across the sensor. The bulk of the literature addressing point sources have demonstrated the concentration plume disperses laterally with a Gaussian structure that widens with downwind distance (Sutton, 1953; Gifford, 1959; Pasquill and Smith, 1983). In the point-source Gaussian (PSG) emission estimation approach described as part of OTM33A, the emission rate of the near-field source is estimated using a Gaussian fit to the wind direction-resolved concentration measurements to establish the peak concentration with plume geometry established by a look-up table reference to ideal dispersion coefficients based on source distance and an estimate of atmospheric stability (Brantley et al., 2014; U.S. EPA, 2014b). The PSG approach does not rely on directly measured lateral plume geometry although some information in this regard is carried in the determination of peak concentrations.

In this paper, two source emission rate calculations are described that use data acquired with OTM 33A or a similar stationary measurement approach. These Gaussian approaches derive the lateral plume geometry by either a model based on wind field information, or by reconstructing the plume using the angle-resolved concentration data. The source emission rates, determined through inversion, for the modeled and reconstructed Gaussian plume approaches are compared with the simple PSG look-up table estimate using data from a series of controlled release trials and field measurements.

## 2. Methods

### 2.1. Measurement approach

The modeled and reconstructed inverse Gaussian source emission rate approaches described here can be used with stationary point measurement data acquired with techniques similar to Draft Method OTM 33A (U.S. EPA, 2014b). This type of measurement produces time-resolved wind field and concentration data that represent observations of a source located 10 m–200 m upwind. The approach is useful for near ground-level sources that are small in spatial extent (point like) and in open environments with absence of trees or obstructions. The technique requires a knowledge of the source location, downwind roadway or fixed fenceline access, and atmospheric conditions conducive to plume advection to the observing location. The primary assumption of this type of observation is that the point sensor is able to obtain an ensemble concentration measurement that is representative of the dispersed source emissions. Since at close range the emitted plume is underdeveloped (filament like, meandering) (Gifford, 1959), sufficient sampling time (on the order of 20 min) is needed to ensure robust (repeated) spatial overlap of plume and sampling probe. Symmetry breaking processes such as flow channeling by obstructions or vertical mismatch of the plume centroid and probe can result in high or low bias in the emission estimate as the primary assumption is violated. In the weak transport limit (low wind speed, very unstable) (Turner, 1994), the adverted plume can largely pass over the fixed sampling probe preventing execution of the measurement (or producing very low bias in the inverse estimate).

Current implementations of OTM 33A use a sport utility vehicle or van fitted with a front-mounted mast with sampling probe and measurement equipment located about 2.5 m above ground level. One or more concentration measurement instruments (CMIs) are located in the vehicle which also carries a battery system to allow instrument operation from stationary locations with the engine turned off. Data presented here are of simulated or actual $CH_4$ emissions with concentration measurements by one of following optical spectroscopic CMIs: a 10 Hz G1301-fc or a 0.5 Hz G1204 (Picarro Inc. Santa Clara, CA, USA), or a 1 Hz GG-24-r (Los Gatos Research, Mountain View CA, USA) CMIs. Additional equipment included a model 81000 3-D sonic anemometer (R.M. Young, Traverse City, Michigan, USA), a model AIO compact auto-north weather station (Climatronics Corp., Bohemia, NY, USA), and a global positioning system (GPS) (Hemisphere GPS Calgary, Alberta, Canada). In mobile form, the vehicle is positioned at the optimal downwind observing location through use of the real-time CMI data ($C_o$) and multiple 20 min stationary measurement sets are acquired with the wind and concentration data time-aligned by a data acquisition program written in LabView™ (National Instruments, Austin TX USA), detailed elsewhere (U.S. EPA, 2014b).

For ONG observations, $CH_4$ is a primary surrogate of product-related emissions. As the spatially underdeveloped $CH_4$ plume meanders on and off the sampling probe, the local $CH_4$ background concentration ($C_b$) is easily established from the $C_o$ time series when using high-precision, 0.5 Hz or faster CMIs, illustrated in Fig. 1. An analysis program, written in MATLAB (MathWorks, Natick MA, USA) calculates $C_b$ as the 5th percentile of the ranked $C_o$ and also performs functions such as compensating for sampling line delay, and rotation of 3D sonic coordinates and calculation of

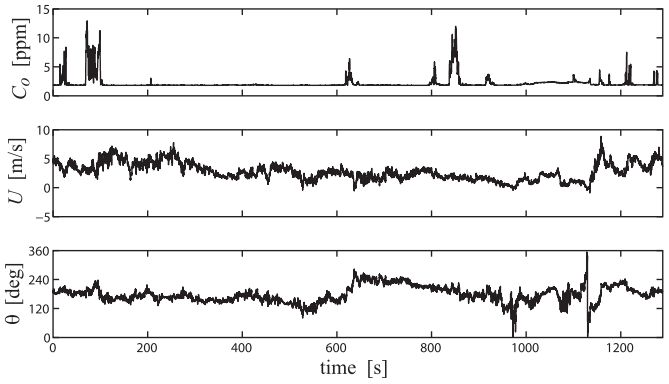


**Fig. 1.** Raw data from controlled release experiment (Wyoming Observation #3) where $C_o$ is methane concentration, $U$ is wind speed, and $\theta$ is wind direction.

atmospheric stability factors used in the PSG emission rate estimate (U.S. EPA, 2014b). All inverse source emission rate calculations presented here are based on the measured concentration above background $C$ where $C = C_o - C_b$.

PSG emission estimate ($S_E$) is a simple 2-D Gaussian integration (no reflection term) calculated as:

$$S_E = 2\pi\sigma_y\sigma_z U_m C_p \tag{1}$$

where $C_p$ is the peak concentration determined by a Gaussian fit, $U_m$ is the mean wind speed, $\sigma_z$ describes the vertical plume height such as $\sigma_y$ defines the lateral plume width. Similar to $\sigma_y$, $\sigma_z$ is determined through look-up tables based on seven levels of atmospheric stability (Brantley et al., 2014).

### 2.2. Controlled releases and data screening

To test OTM 33A and other mobile and fixed-place emissions detection and measurement approaches, controlled release (CR) trials that simulate leaks are performed (U.S. EPA, 2014b; Rella et al., 2015; EDF, 2015). EPA has conducted a total of 106 $CH_4$ CR trials that attempt to simulate OTM 33A-observable emissions from ONG production pads in a variety of conditions, detailed elsewhere (U.S. EPA, 2014b; Brantley et al., 2014). OTM 33A and similar near-field stationary point measurement approaches attempt to minimize implementation burden so no site-specific modeling or tracer gas is used. The approach instead attempts to flag and remove results that may contain significant method error through use of data quality indicators (DQIs). For this initial discussion of two Gaussian plume inverse approaches, a set of DQIs is described that yield 39% of the current CR trials which were largely conducted in North Carolina generally under less than ideal advected transport conditions. A total of seven field observations from Wyoming under significantly different transport are included to assist in comparison. These DQIs are described in Section 2.4 after introduction of terms.

Tables 1 and 2 summarize the CR and Wyoming data sets respectively used for this analysis. These tables provide the date of the measurement, the measurement distance from the source ($L_x$), the source height ($z_s$), the mean wind speed ($U_m$), the standard deviation of the wind direction ($\sigma_\theta$), and the wind direction at the peak average concentration ($\theta_p$). For the CR files, the known release rate ($S_o$) and the OTM 33A PSG emission rate estimate ($S_E$) are also provided. The CR rates were monitored either by a calibrated mass flow sensor or a rotameter and manually adjusted to maintain the release rates near the target value. The actual release rates are within ±5% of target (Brantley et al., 2014).

### 2.3. Theory and calculation

We seek to develop a conditional sampling strategy that will help describe a plume's transverse structure. The ensemble mean downwind concentration distribution is typically represented in dispersion models as a function of downwind distance ($x$), crosswind position ($y$), and height ($z$) as shown:

$$C_m(x,y,z) = S\frac{D_y(x,y)D_z(x,z)}{\overline{U}} \tag{2}$$

where $S$ is the source strength, $\overline{U}$ is the effective speed of plume advection, and $D_y(x,y)$ and $D_z(x,z)$ are the crosswind and vertical dispersion factors, respectively (Horst and Weil, 1992). $C_m(x,y,z)$ is the ensemble mean above background $CH_4$ concentration data modeled at a height $z$, a distance $x$ downwind, and at the crosswind position $y$ from the plume center. In this study, we want to determine $S$ associated with the conditional mean concentration of the $CH_4$ data measured downwind. We assume a near-ground source emitted continuously with a relatively constant wind speed (Table 1).

The plume advective speed ($\overline{U}$) is computed at the effective height of the plume ($\bar{z}$):

$$\overline{U} = U(\bar{z}) = \frac{u_*}{\kappa}\left[\ln\left(\frac{c\bar{z}}{z_o}\right) - \Psi\left(\frac{c\bar{z}}{L}\right)\right] \tag{3}$$

where $z_o$ is the momentum roughness length, $c$ is a constant set to 0.6, $u_*$ is the friction velocity, $L$ is the Monin-Obukhov length, and $\Psi$ is a dimensionless stability function estimated from the Businger-Dyer formula (see Appendix A for $z_o$, $u_*$, $L$, and $\Psi$ calculation) (Dyer, 1974; Gryning et al., 1983; Monin and Obukhov, 1954). Note that $z_o$ is calculated from properties of the wind profile (Monin and Obukhov, 1954).

As the plume moves downwind, it spreads both laterally and vertically where $D_z$ describes the vertical dispersion. By assuming the vertical eddy diffusivity and wind speed are approximated by a power law, $D_z$ is calculated as expressed by (van Ulden, 1978):

$$D_z(x,z) = \frac{A}{\bar{z}}\exp\left[-\left(\frac{Bz}{\bar{z}}\right)^s\right] \tag{4}$$

where $z$ is the measurement height ($z = z_m$), $s$ is a shape parameter, and $A$ and $B$ are functions of $s$ (see Appendix A for s, A, and B calculation) (Gryning et al., 1987). CR results of this study are based on a known location and height of the source with only one possible source as $\bar{z}$ is a function of the source height $z_s$ and source location $L_x$ (Appendix A). In the field, these values are unknown with the possibility of multiple sources which can increase uncertainty in the source strength estimate. To help reduce uncertainty, the OTM 33A mobile measurement technique utilizes infrared cameras to help determine which source is leaking and approximates the location using GPS and satellite imagery (U.S. EPA, 2014b).

The crosswind plume profile due to dispersion from a continuous point source is shown to resemble a Gaussian distribution (Gryning et al., 1987), with:

$$D_y(x,y) = \frac{1}{\sqrt{2\pi}\sigma_y}\exp\left[-\frac{1}{2}\left(\frac{y}{\sigma_y}\right)^2\right] \tag{5}$$

where $\sigma_y$ defines the width of the plume such as $\sigma$ defines the standard deviation of a Gaussian distribution.

Using sonic anemometer measurements, values $L$, $u_*$, $\bar{z}$, $s$, $\Psi$, and $z_o$ are calculated as shown in Appendix A. From these values, $D_z$ and $\overline{U}$ are calculated (Gryning et al., 1987; van Ulden, 1978). $C$ is

**Table 1**
Summary of meteorological conditions during the CR experiments that were used to estimate the source strength including effective wind speed ($\overline{U}$), and mean wind speed ($U_m$). $S_o$ is the known release rate. $S_M$ and $S_R$ are this method's calculated source strengths. $S_E$ is calculated using OTM 33A PSG method.

| Obs.# | Date | $L_x$(m) | $z_s$(m) | $z/L(-)$ | $\overline{U}$(m/s) | $U_m \pm \sigma_U$(m/s) | $\sigma_\theta$(deg) | $\theta_p$(deg) | $\langle C\|\theta_p\rangle$(ppm) | $S_o$(g/s) | $S_M$(g/s) | $S_R$(g/s) | $S_E$(g/s) |
|---|---|---|---|---|---|---|---|---|---|---|---|---|---|
| 1 | 05/22/10 | 18 | 1.5 | −0.11 | 1.6 | 2.4 ± 0.8 | 34 | 214 | 6.0 | 0.60 | 0.46 | 0.48 | 0.49 |
| 2 | 11/12/10 | 46 | 1.5 | −0.18 | 2.3 | 2.0 ± 1.0 | 44 | 184 | 0.9 | 0.60 | 0.27 | 0.30 | 0.53 |
| 3 | 11/12/10 | 33 | 1.5 | −0.08 | 1.8 | 1.7 ± 0.9 | 49 | 150 | 7.0 | 0.60 | 0.37 | 0.44 | 1.05 |
| 4 | 04/20/11 | 40 | 3.1 | −0.05 | 3.4 | 3.3 ± 1.5 | 30 | 150 | 2.1 | 0.60 | 0.57 | 0.62 | 0.52 |
| 5 | 04/20/11 | 60 | 3.1 | −0.05 | 2.8 | 2.6 ± 1.1 | 29 | 189 | 1.5 | 0.60 | 0.63 | 0.65 | 0.56 |
| 6 | 04/20/11 | 35 | 3.1 | −0.01 | 2.6 | 2.6 ± 1.2 | 34 | 218 | 4.1 | 0.60 | 0.69 | 0.73 | 0.81 |
| 7 | 04/20/11 | 57 | 3.1 | −0.04 | 3.4 | 3.4 ± 1.2 | 28 | 160 | 0.7 | 0.60 | 0.40 | 0.48 | 0.39 |
| 8 | 05/06/11 | 88 | 3.1 | −0.08 | 3.8 | 3.3 ± 1.0 | 25 | 188 | 0.6 | 0.60 | 0.47 | 0.50 | 0.61 |
| 9 | 05/06/11 | 88 | 3.1 | −0.07 | 3.8 | 3.3 ± 1.3 | 20 | 180 | 0.6 | 0.60 | 0.73 | 0.65 | 0.66 |
| 10 | 05/06/11 | 98 | 3.1 | −0.06 | 3.7 | 3.1 ± 1.4 | 26 | 203 | 0.4 | 0.60 | 0.43 | 0.45 | 0.39 |
| 11 | 05/06/11 | 98 | 3.1 | −0.03 | 4.8 | 4.0 ± 1.5 | 23 | 189 | 0.6 | 0.60 | 0.79 | 0.73 | 0.81 |
| 12 | 05/06/11 | 103 | 3.1 | −0.03 | 4.4 | 3.8 ± 1.6 | 26 | 157 | 0.6 | 0.60 | 0.59 | 0.61 | 0.73 |
| 13 | 05/06/11 | 82 | 3.1 | −0.03 | 2.6 | 2.2 ± 1.0 | 27 | 197 | 1.1 | 0.60 | 0.77 | 0.69 | 0.62 |
| 14 | 05/06/11 | 57 | 3.1 | −0.12 | 2.8 | 2.7 ± 1.0 | 31 | 203 | 3.8 | 0.60 | 0.52 | 0.62 | 0.75 |
| 15 | 04/20/11 | 40 | 3.1 | −0.06 | 3.3 | 3.3 ± 1.5 | 30 | 155 | 3.8 | 0.60 | 0.58 | 0.60 | 0.63 |
| 16 | 04/20/11 | 60 | 3.1 | −0.06 | 2.8 | 2.5 ± 1.0 | 29 | 187 | 1.4 | 0.60 | 0.61 | 0.67 | 0.61 |
| 17 | 04/20/11 | 35 | 3.1 | −0.02 | 2.6 | 2.6 ± 1.2 | 34 | 223 | 4.7 | 0.60 | 0.54 | 0.62 | 0.64 |
| 18 | 04/20/11 | 97 | 3.1 | −0.04 | 3.8 | 3.5 ± 1.2 | 22 | 163 | 0.9 | 0.60 | 0.29 | 0.34 | 0.31 |
| 19 | 04/20/11 | 57 | 3.1 | −0.02 | 3.4 | 3.3 ± 1.2 | 29 | 147 | 1.2 | 0.60 | 0.42 | 0.52 | 0.46 |
| 20 | 05/06/11 | 88 | 3.1 | −0.14 | 3.7 | 3.4 ± 1.0 | 23 | 153 | 0.4 | 0.60 | 0.20 | 0.20 | 0.47 |
| 21 | 05/06/11 | 88 | 3.1 | −0.15 | 3.5 | 3.0 ± 1.2 | 23 | 187 | 0.7 | 0.60 | 0.73 | 0.75 | 0.57 |
| 22 | 05/06/11 | 98 | 3.1 | −0.07 | 3.8 | 3.3 ± 1.5 | 26 | 204 | 0.4 | 0.60 | 0.42 | 0.42 | 0.49 |
| 23 | 05/06/11 | 98 | 3.1 | −0.04 | 4.6 | 4.1 ± 1.5 | 24 | 207 | 0.8 | 0.60 | 0.68 | 0.65 | 0.71 |
| 24 | 05/06/11 | 103 | 3.1 | −0.03 | 4.4 | 3.7 ± 1.6 | 27 | 168 | 0.6 | 0.60 | 0.69 | 0.73 | 0.66 |
| 25 | 05/06/11 | 82 | 3.1 | −0.03 | 2.6 | 2.2 ± 1.0 | 25 | 185 | 1.0 | 0.60 | 0.69 | 0.67 | 0.57 |
| 26 | 05/06/11 | 57 | 3.1 | −0.15 | 2.8 | 2.7 ± 1.0 | 29 | 225 | 2.1 | 0.60 | 0.73 | 0.89 | 1.02 |
| 27 | 06/05/12 | 51 | 3.1 | −0.12 | 2.7 | 2.5 ± 0.9 | 29 | 153 | 1.7 | 0.70 | 0.64 | 0.70 | 0.62 |
| 28 | 06/05/12 | 39 | 3.1 | −0.16 | 3.3 | 3.1 ± 0.9 | 21 | 192 | 2.5 | 0.70 | 0.95 | 0.86 | 0.70 |
| 29 | 06/05/12 | 67 | 3.1 | −0.17 | 3.1 | 2.6 ± 0.9 | 24 | 181 | 1.2 | 0.70 | 0.75 | 0.72 | 0.68 |
| 30 | 06/05/12 | 19 | 3.1 | −0.13 | 3.4 | 3.4 ± 1.4 | 29 | 171 | 7.1 | 0.70 | 1.23 | 0.92 | 0.95 |
| 31 | 06/05/12 | 29 | 3.0 | −0.20 | 3.1 | 3.0 ± 1.0 | 30 | 211 | 6.4 | 1.20 | 0.89 | 0.95 | 0.82 |
| 32 | 07/11/12 | 106 | 3.1 | 0.02 | 2.2 | 1.9 ± 0.9 | 63 | 195 | 0.9 | 0.70 | 0.54 | 0.54 | 0.89 |
| 33 | 05/08/13 | 41 | 1.5 | −0.16 | 1.6 | 1.5 ± 0.7 | 45 | 193 | 0.8 | 0.19 | 0.16 | 0.16 | 0.19 |
| 34 | 05/09/13 | 52 | 3.1 | −0.10 | 2.7 | 2.5 ± 1.0 | 33 | 200 | 1.4 | 0.60 | 0.71 | 0.75 | 0.63 |
| 35 | 05/09/13 | 52 | 3.1 | −0.15 | 2.4 | 2.0 ± 0.9 | 41 | 176 | 1.1 | 0.60 | 0.55 | 0.59 | 0.58 |
| 36 | 05/13/13 | 54 | 3.1 | −0.13 | 3.7 | 3.5 ± 1.3 | 33 | 142 | 0.5 | 0.60 | 0.32 | 0.38 | 0.39 |
| 37 | 05/13/13 | 18 | 3.1 | −0.10 | 1.9 | 1.9 ± 1.2 | 62 | 155 | 2.5 | 0.60 | 0.41 | 0.46 | 0.30 |
| 38 | 05/14/13 | 35 | 1.5 | −0.19 | 2.0 | 1.9 ± 1.0 | 57 | 215 | 1.2 | 0.19 | 0.22 | 0.24 | 0.49 |
| 39 | 05/15/13 | 44 | 3.1 | −0.09 | 2.4 | 2.3 ± 0.9 | 32 | 209 | 0.6 | 0.19 | 0.14 | 0.16 | 0.20 |
| 40 | 05/15/13 | 43 | 3.1 | −0.08 | 2.3 | 2.1 ± 0.9 | 28 | 205 | 0.7 | 0.19 | 0.23 | 0.23 | 0.20 |
| 41 | 05/15/13 | 43 | 3.1 | −0.13 | 2.2 | 2.0 ± 0.9 | 36 | 202 | 0.7 | 0.19 | 0.22 | 0.23 | 0.28 |

measured at only one location yet Eq. (2) shows $C_m$ as a function of $x$, $y$, and $z$. This study uses the wind direction to reconstruct the plume's transverse structure in order to estimate the crosswind position $y$, and in turn calculate $\sigma_y$ and $D_y$.

### 2.3.1. Conditionally averaged concentration

Over the observation period, each concentration measurement coincides with a wind direction measurement. When the wind is directed toward the sensor, the measured concentration represents the center of the plume ($y = 0$). When the wind is directed away from the sensor, the measured concentration represent the plume at a crosswind position.

During data analysis, the concentration values are organized based on the wind direction where multiple concentration values are obtained within a given instantaneous wind direction range. An ensemble Gaussian plume is constructed by calculating a conditionally averaged concentration value within a given wind direction range. The conditionally averaged concentration value, denoted $\langle C|\theta\rangle$, is calculated within designated wind angle increments ($\Delta\theta$) as shown:

$$\langle C|\theta\rangle = \frac{1}{n}\sum_{\theta_i \in \Theta(\theta)} C(\theta_i) \tag{6}$$

where $\Theta(\theta) = \{\theta_i : |\theta_i - \theta| \le \Delta\theta/2,\ \forall i = 1, \ldots, n\}$, and $n$ is the total number of data points within the given $\Theta$. $\Delta\theta$ is set at 2°. Note that if $\Delta\theta$ is too large, $\langle C|\theta\rangle$ values are decreased and may impact the source strength calculation. However, $\Delta\theta$ is necessary as it accounts for

**Table 2**
Summary of meteorological conditions during the Wyoming field studies that were used to estimate the source strength. $S_M$ and $S_R$ are this method's calculated source strengths. $S_E$ is calculated using OTM 33A PSG method.

| Study# | Date | $L_x$(m) | $z_s$(m) | $z/L(-)$ | $\overline{U}$(m/s) | $U_m \pm \sigma_U$(m/s) | $\sigma_\theta$(deg) | $\theta_p$(deg) | $\langle C\|\theta_p\rangle$(ppm) | $S_M$(g/s) | $S_R$(g/s) | $S_E$(g/s) |
|---|---|---|---|---|---|---|---|---|---|---|---|---|
| 1 | 06/16/11 | 42 | 3.1 | −0.15 | 2.7 | 2.4 ± 1.0 | 43 | 167 | 6.4 | 3.22 | 3.42 | 1.29 |
| 2 | 06/16/11 | 51 | 3.1 | −0.14 | 3.6 | 3.2 ± 1.3 | 44 | 187 | 4.4 | 3.50 | 3.32 | 2.57 |
| 3 | 06/16/11 | 60 | 3.1 | −0.13 | 3.6 | 3.2 ± 1.5 | 34 | 202 | 1.4 | 1.05 | 1.20 | 0.88 |
| 4 | 06/16/11 | 86 | 3.1 | −0.05 | 3.8 | 3.2 ± 1.6 | 66 | 140 | 4.7 | 5.45 | 7.55 | 7.29 |
| 5 | 06/16/11 | 36 | 3.1 | −0.09 | 5.0 | 4.9 ± 1.4 | 19 | 170 | 2.4 | 1.49 | 1.38 | 0.49 |
| 6 | 06/16/11 | 60 | 3.1 | −0.03 | 7.1 | 6.7 ± 1.7 | 16 | 166 | 3.6 | 5.37 | 5.36 | 2.33 |
| 7 | 06/16/11 | 73 | 3.1 | −0.06 | 6.6 | 6.1 ± 1.4 | 15 | 200 | 0.6 | 0.73 | 0.68 | 0.38 |

possible error associated with wind direction measurements as the true $\theta$ may lie within $\pm\Delta\theta$. This error is because the local, instantaneous wind direction is assumed representative of the average wind direction over the travel distance from the source to the sensor. $\langle C|\theta\rangle$ is calculated for each $\theta$ ranging from 0° to 360° at an increment of 2°. OTM 33A PSG uses the maximum $\langle C|\theta\rangle$ to calculate the source strength and discards the other points from analysis.

### 2.3.2. Plume geometry

Although $C$ is measured at a stationary position, the wind direction $\theta$ can be used to reconstruct the plume shape and provide an estimated crosswind position $y$ ($\widehat{Y}$). Using the geometric relationship shown in Fig. 2, each $\theta$ data point associated with $\langle C|\theta\rangle$ is converted to $\widehat{Y}$ as shown:

$$\widehat{Y}(\theta) = L_x \sin(\theta - \theta_p) \tag{7}$$

where $L_x$ is the distance from the sensor to the source, and $\theta_p$ is the wind direction associated with the plume center (Fig. 3). In this study, $L_x$ is a measured value, and $\theta_p$ is calculated as:

$$\theta_p = \underset{\theta}{\operatorname{argmax}} \langle C|\theta\rangle \tag{8}$$

for each file. During measurement, the sonic anemometer is directed toward the source so that $\theta_p$ should be ~180°.

The length scale $\sigma_y$ is classically determined using similarity theory:

$$\sigma_{y,M} = a_y z_o 1.9 \left(\frac{L_x}{z_0}\right)^{p_y} \tag{9}$$

where constants $a_y$ and $p_y$ are functions of atmospheric stability (Eckman, 1994). The OTM 33A PSG method determines $\sigma_y$ from a look-up table based on seven levels of atmospheric stability. In this study, $\sigma_y$ is calculated using the plume reconstructed lateral geometry:

$$\sigma_{y,R} = \sqrt{\frac{1}{N}\sum_{i=1}^{N} \widehat{Y}_i'^2}; \tag{10}$$

where $N$ is the number of $\langle C|\widehat{Y\prime}\rangle$ values, and $\widehat{Y\prime}$ are the $\widehat{Y}$ values where $\langle C|\widehat{Y}\rangle$ is greater than a minimum concentration ($C_{\min}$) and measured within ±40° off the plume center. The ±40° threshold focuses the $\sigma_{y,R}$ calculation to the plume center while the minimum concentration ensures the concentration values are well above background. In practice, the minimum concentration is estimated as the 75th percentile of the ranked $C$.

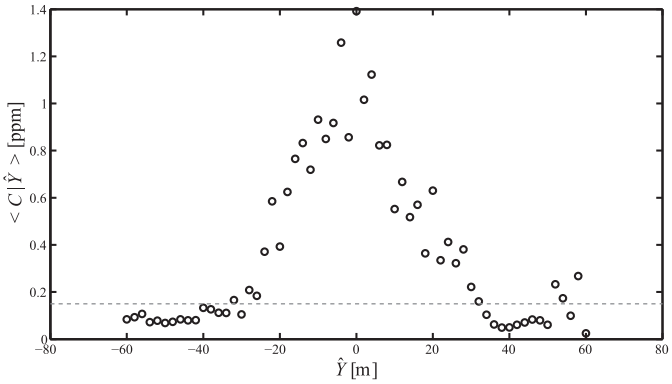


**Fig. 3.** Reconstructed plume of concentration $C$ values as a function of estimated distance to plume center ($\widehat{Y}$) for Wyoming Observation # 3 where the dashed line represents the minimum concentration $C_{\min}$. All values below $C_{\min}$ are not included in the calculation of the plume width $\sigma_{y,R}$.

The two calculated $\sigma_y$ are compared to see the effect of estimating $\sigma_{y,M}$ from atmospheric stability and $\sigma_{y,R}$ from the plume lateral structure (Fig. 4). These values are used to calculate two $D_y$ ($D_{y,M}$ and $D_{y,R}$) from Eq. (5) which results in two respective $S$ estimates ($S_M$ and $S_R$). For the CR experiments, $\sigma_{y,M}$ and $\sigma_{y,R}$ are correlated with an $R^2 = 0.63$ correlation, and a mean square error (MSE) of 21.21.

### 2.3.3. Source strength

With a known $S$, the downwind ensemble mean concentration can be modeled (Eq. (2)). However in this study, $S$ is unknown and the measured concentration is used to estimate $S$. The source strength estimated by OTM 33A PSG method ($S_E$) is calculated as shown in Eq. (1). In this study, we are able to estimate $S$ from Eq. (2) in a least-squares sense with the origin fixed at zero:

$$S = \frac{\sum_{i=1}^{N} \frac{D_y D_z}{U} \left\langle C\middle|\widehat{Y}_i\right\rangle}{\sum_{i=1}^{N} \left(\frac{D_y D_z}{U}\right)^2} \tag{11}$$

where $\sigma_y$ ($\sigma_{y,M}$,$\sigma_{y,R}$) are used to estimate $S$ ($S_M$,$S_R$), respectively. For both $S_M$ and $S_R$ calculation, we focus on the center of the plume so that only the $\langle C|\widehat{Y}\rangle$ values within ±40° of the plume center are used in the source strength estimation. In order to examine the

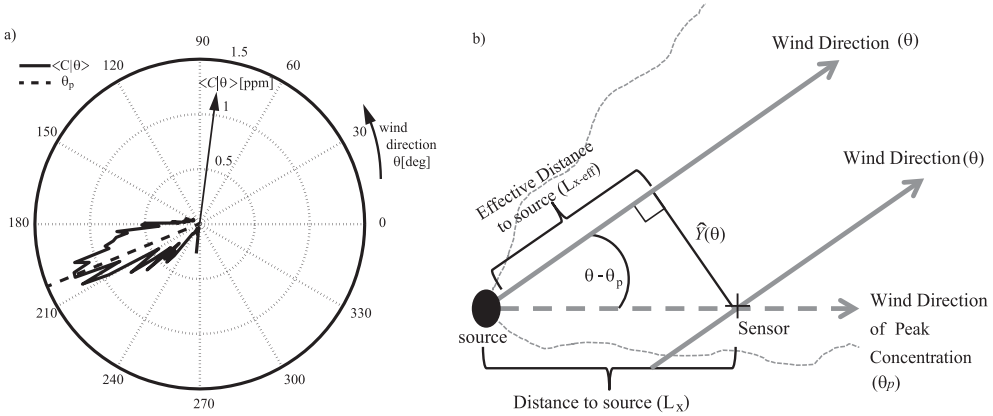


**Fig. 2.** (a) Polar plot with conditionally average concentration $\langle C|\theta\rangle$ as the distance from the center and the wind direction $\theta$ as the radial axis for Wyoming Observation # 3. The peak wind direction $\theta_p$ is shown at the maximum $\langle C|\theta\rangle$. (b) Schematic of wind direction geometry for converting $\theta$ to estimated crosswind position $\widehat{Y}$. The dashed lines represent the source plume.

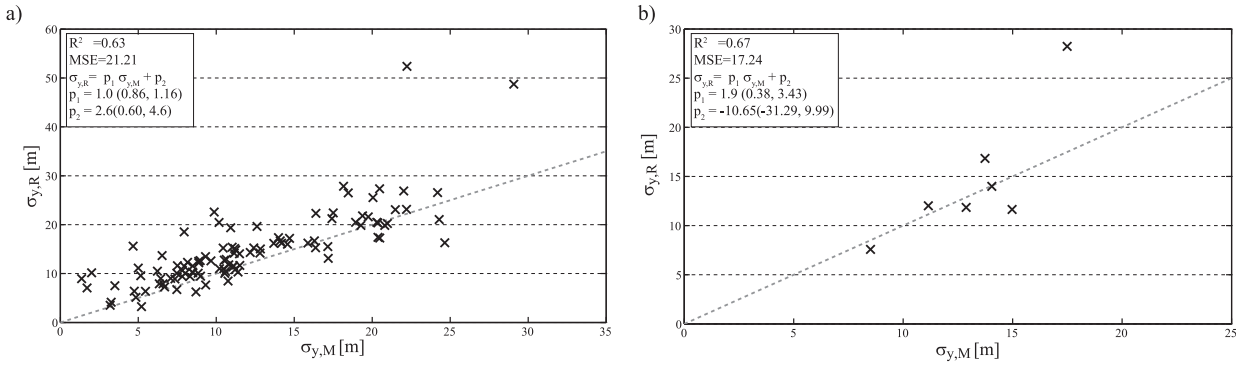


**Fig. 4.** Comparison of calculated plume width $\sigma_y$ values for each (a) CR file and (b) Wyoming file where $\sigma_{y,M}$ is calculated from atmospheric stability and $\sigma_{y,R}$ calculated from the reconstructed plume geometry. The dashed line is a line with a slope of 1 and an intercept of 0. The regression statistics are shown with the coefficients 95% confidence interval shown in parentheses.

difference of estimated source strength due to the particular $\sigma_y$, the source strengths $S_M$ and $S_R$ are compared for both the CR and Wyoming observations (Fig. 5). For CR observations, $S_M$ and $S_R$ have a linear relationship with an $R^2 = 0.91$ correlation, and a MSE of 0.004. For field studies, Fig. 5b shows an $R^2 = 0.93$ correlation between $S_M$ and $S_R$ and a MSE of 0.55.

Percent error is used to understand the accuracy of the Gaussian-reconstruction method. The percent error ($\varepsilon$) of the CR measurements is calculated for each observation:

$$\varepsilon = \frac{S - S_o}{S_o} \times 100 \tag{12}$$

where a ±5% error is associated with the known $S_o$.

### 2.4. Data assessment

For this analysis, the primary causes for data quality issues are due to (1) non-neutral atmospheric transport conditions (Monin and Obukhov, 1954), (2) low $CH_4$ signal, (3) partial capture of the plume structure on-axis case, and (4) partial capture of the plume structure off-axis case. Four transport DQIs unique to this analysis are implemented to identify these data quality issues: (1) absolute value of stability ($|z/L|$) less than 0.2; (2) $\langle C|\theta_p\rangle$ greater than 0.3 ppm; (3) the standard deviation of wind direction ($\sigma_\theta$) greater than 20°; and (4) $\theta_p$ within 180±50°. Only observations that pass all four DQIs are used in this analysis; 51 out of 106 files were flagged due to stability DQI, 11 flagged by the peak average concentration DQI, 10 flagged by the standard deviation of wind direction DQI, and 10 flagged by the fitted peak direction (some flagged by multiple DQIs) leaving a total of 41 for further analysis.

The stability parameter DQI flags data measured in the unstable atmosphere ($z/L < 0.2$) as well as the stable atmosphere ($z/L > 0.2$) where the neutral atmosphere is defined in this analysis by $|z/L| < 0.2$. Unstable conditions can lead to an underestimate of $S$ as the plume may rise above the sensor and therefore the ensemble concentration measurement is not representative of the dispersed source emissions. Stable conditions can lead to an overestimate of $S$ as the vertical dispersion (Eq (4)) and effective wind speed (Eq. (A.8)) equations are shown to have increased error in stable conditions (van Ulden, 1978). CR observations with $|z/L| < 0.2$ have an $\varepsilon$ range of −97–165 % and therefore flags the two extremes of under and overestimated source strengths.

$\langle C|\theta_p\rangle$ less than 0.3 ppm indicates a weak plume signal that could be do to insufficient plume transport or poor plume-probe overlap. Low $\langle C|\theta_p\rangle$ tends to underestimate the source strength; CR observations with $\varepsilon < -80$ % have a $\langle C|\theta_p\rangle$ mean value of 0.5 ppm. In contract, CR observations with $|\varepsilon| = 5\%$ have a $\langle C|\theta_p\rangle$ mean value of 2.1 ppm with a standard deviation of 1.7 ppm. Out of 106 observations, 11 have $\langle C|\theta_p\rangle$ values less than 0.3 ppm where 9 out of the 11 observations are underestimated by at least 31%. The percent error for these 11 observations ranges from −92% to 11% with an average error of −41% and a standard deviation of 32%.

Wind direction variance plays an important roll in stationary measurement approaches since sufficient mean wind direction change during the observation is required capture the full plume geometry. Low wind direction variance can lead to overestimation in some cases. The standard deviation of the wind direction $\sigma_\theta$ is

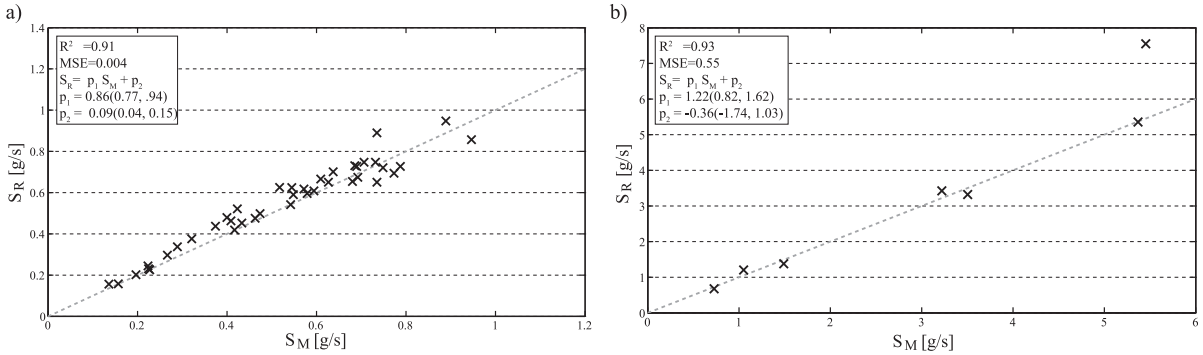


**Fig. 5.** Comparison of the two estimated source strength for each (a) CR file and (b) Wyoming file where $S_M$ is estimated with the plume width $\sigma_{y,M}$ calculated from atmospheric stability and $S_R$ is estimated with the plume width $\sigma_{y,R}$ calculated from the reconstructed plume geometry. The dashed line is a line with a slope of 1 and an intercept of 0. The regression statistics are shown with the coefficients 95% confidence interval shown in parentheses.

used to quantify the variation of the wind direction during the stationary observation period. CR observations that are greatly overestimated ($\varepsilon > 80$ %) have a $\sigma_\theta$ mean value of 25 deg. When the standard deviation is low, only the center (on-axis) of the plume is captured during the measurement. Out of 106 observations, 10 have $\sigma_\theta$ values less than 20° where 6 out of the 10 observations are overestimated by at least 30%. The percent error for these 10 observations ranges from −12% to 95% with an average error of 33% and a standard deviation of 30%.

The mean wind direction during the measurement must be relatively well aligned with the observation location or the plume may miss laterally. Restricting observations to $\theta_p$ within 180±50° identifies possible errors due to capturing only off-axis concentration measurements when the mean wind is not directed toward the sensor. CR observations with $|\varepsilon| = 5\%$ have a $\theta_p$ of 176° with a standard deviation of 30 deg. Out of 106 observations, 10 have $\theta_p$ values outside 180±50° where 8 out of the 10 observations are underestimated by at least 28%. The percent error for these 10 observations ranges from −92% to 30% with an average error of −41% and a standard deviation of 38%.

## 3. Results and discussion

### 3.1. Source strength results

The source strength results represent all 7 Wyoming field studies and only the 41 CR observations (14 studies) that pass all four DQIs (Tables 1 and 2). For CR, a study is defined by measurements that occurred on the same day and from the same CR set-up which includes the same $S_o$ and CMI. CR measurements were made between 18 and 106 m downwind of the source; Wyoming measurements were made between 36 and 86 m $S_M$, $S_R$, $S_E$ are compared to $S_o$ for CR files only (Fig. 6). For the Wyoming field studies, $S_R$ is compared to $S_E$.

Fig. 7 shows the distribution of the percent error for $S_M$ (left), $S_R$ (center), and $S_E$ (right). The mean percent error for $S_M$, $S_R$, and $S_E$ are −5%, -2%, and 6% with a standard deviation of 29%, 25%, and 37%, respectively. The mean percent error results show the $S_M$ and $S_R$ results tend to be underestimated while the $S_E$ results tend to be overestimated. The percent error ranges from −70 to 75 %, -70 to 48 %, and −50 to 160 % for $S_M$, $S_R$, and $S_E$, respectively. Note that DQIs for $S_E$ used in this analysis differ than other approaches (Brantley et al., 2014; U.S. EPA, 2014b). When looking at the magnitude of the percent error, the average absolute percent error for $S_M$, $S_R$, and $S_E$ is calculated as 24%, 20%, and 24%, respectively. Observations where all three methods underestimate S (e.g. Observation 18) may be due to the plume passing over the sensor where the sensor measures only the bottom of the plume.

The three methods are compared to each other by determining

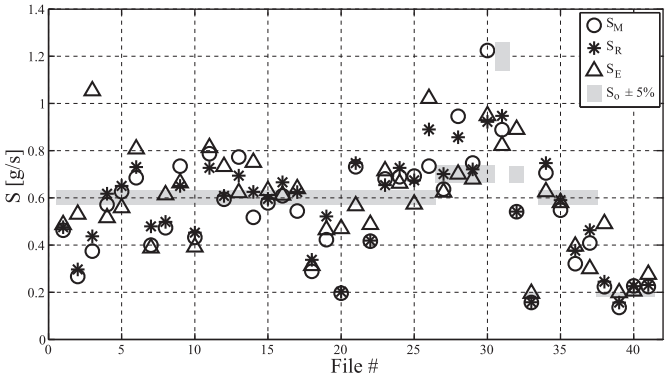


**Fig. 6.** Calculated source strength ($S_M$, $S_R$, and $S_E$) for each CR file.

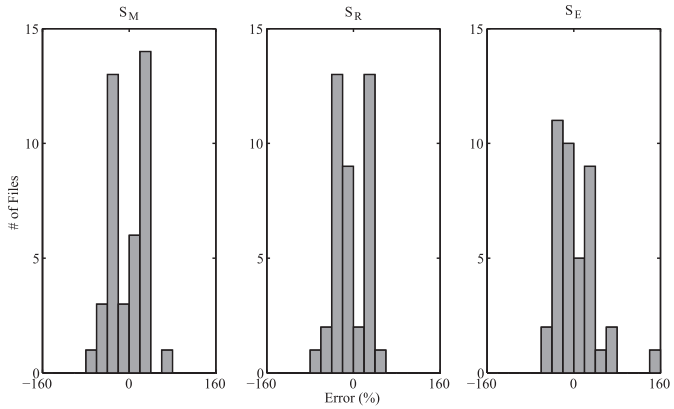


**Fig. 7.** Percent error in the estimated source strengths ($S_M$, $S_R$, and $S_E$) for each CR study.

the percent difference (PD):

$$PD = \frac{|S_i - S_j|}{\frac{1}{2}(S_i + S_j)} \times 100 \tag{13}$$

where $S_i$ and $S_j$ are $S_M$, $S_R$, or $S_E$. The three methods have a $PD < 30$ % for 78% of all 41 CR observations. All $S_M$ and $S_R$ estimates have a $PD < 30$ % of each other and 80% of the 41 CR observations agree within 15% of each other. There are two observations (observations 3 and 20) with $PD > 80$ % when comparing the $S_M$ and $S_R$ to $S_E$.

The source strength is determined and analyzed for all seven Wyoming field studies. As evidenced in Table 2, $S_M$ and $S_R$ have a $PD < 32$ % for all seven studies with an average $PD = 10$ %. However, there is a systematic difference in $S_M$ and $S_R$ to $S_E$ where $S_M$ and $S_R$ are consistently greater than $S_E$ for all seven studies with a $PD$ up to 101%. Table 2 shows that 3 out of the 7 studies would not pass the four DQI as $\sigma_\theta < 20$ deg. These three sites also have a high wind speed ranging from 4.9 to 6.7 m/s which is higher than all the CR measurements. For these sites, the $PD$ between $S_M$ and $S_R$ to $S_E$ is less than 57% with an average $PD = 79$ % while those that pass the four DQI have an average $PD = 40\%$.

The impact of multiple measurements made for a given source is analyzed by calculating the average source strength $\overline{S}$ for each study ($i$):

$$\overline{S_i} = \frac{1}{n_i}\sum_{k=1}^{n_i} S_k \tag{14}$$

where $n_i$ is the number of files within the given study and $\overline{S_i}$ is calculated separately for $S_M$, $S_R$, and $S_E$. Table 3 and Fig. 8 shows the percent error for $\overline{S}$ results ranges from −47 to 27 %, -39 to 29 %, and −42 to 158 % for $\overline{S_M}$, $\overline{S_R}$, and $\overline{S_E}$, respectively. The largest ∈ occurs when there are less than 3 files within the given study. These results suggest multiple measurements help reduce the error in the source strength estimate.

## 4. Conclusions

Development of cost effective inspection approaches to detect and assess fugitive emissions from upstream ONG production operations can support environmentally responsible development and save money through reduced product loss. EPA draft method OTM 33A and similar stationary approaches observe emissions from remote vantage points using either mobile or permanent fenceline sensors. These approaches require robust inverse source algorithms to be effective. This work contributes to this developing

**Table 3**
CR mean source strength results and the average percent error ($\varepsilon$), the source strength standard deviation ($\sigma$) shown in parenthesis for each study where $n_i$ is the number of observations within the given study.

| Study | Date | $S_o$(g/s) | $S_M$ ($\sigma_M$) (g/s) | Error (%) | $S_R$ ($\sigma_R$) (g/s) | Error (%) | $S_E$ ($\sigma_E$) (g/s) | Error (%) | $n_i$(#) |
|---|---|---|---|---|---|---|---|---|---|
| 1 | 05/22/10 | 0.6 | 0.46 (0.00) | −23% | 0.48 (0.00) | −21% | 0.49 (0.00) | −19% | 1 |
| 2 | 11/12/10 | 0.6 | 0.32 (0.08) | −47% | 0.37 (0.10) | −39% | 0.79 (0.37) | 32% | 2 |
| 3 | 04/20/11 | 0.6 | 0.57 (0.12) | −5% | 0.62 (0.10) | 3% | 0.57 (0.18) | −5% | 4 |
| 4 | 05/06/11 | 0.6 | 0.62 (0.15) | 3% | 0.61 (0.10) | 1% | 0.65 (0.14) | 9% | 7 |
| 5 | 04/20/11 | 0.6 | 0.49 (0.13) | −18% | 0.55 (0.13) | −9% | 0.53 (0.14) | −11% | 5 |
| 6 | 05/06/11 | 0.6 | 0.59 (0.21) | −1% | 0.62 (0.23) | 3% | 0.64 (0.19) | 7% | 7 |
| 7 | 06/05/12 | 0.7 | 0.89 (0.26) | 27% | 0.80 (0.11) | 14% | 0.74 (0.14) | 5% | 4 |
| 8 | 06/05/12 | 1.2 | 0.89 (0.00) | −26% | 0.95 (0.00) | −21% | 0.82 (0.00) | −32% | 1 |
| 9 | 07/11/12 | 0.7 | 0.54 (0.00) | −23% | 0.54 (0.00) | −23% | 0.89 (0.00) | 27% | 1 |
| 10 | 05/08/13 | 0.19 | 0.16 (0.00) | −17% | 0.16 (0.00) | −17% | 0.19 (0.00) | 2% | 1 |
| 11 | 05/09/13 | 0.6 | 0.63 (0.11) | 5% | 0.67 (0.11) | 12% | 0.60 (0.03) | 0% | 2 |
| 12 | 05/13/13 | 0.6 | 0.36 (0.06) | −39% | 0.42 (0.06) | −30% | 0.35 (0.07) | −42% | 2 |
| 13 | 05/14/13 | 0.19 | 0.22 (0.00) | 18% | 0.24 (0.00) | 29% | 0.49 (0.00) | 158% | 1 |
| 14 | 05/15/13 | 0.19 | 0.20 (0.05) | 8% | 0.23 (0.04) | 19% | 0.23 (0.04) | 19% | 3 |

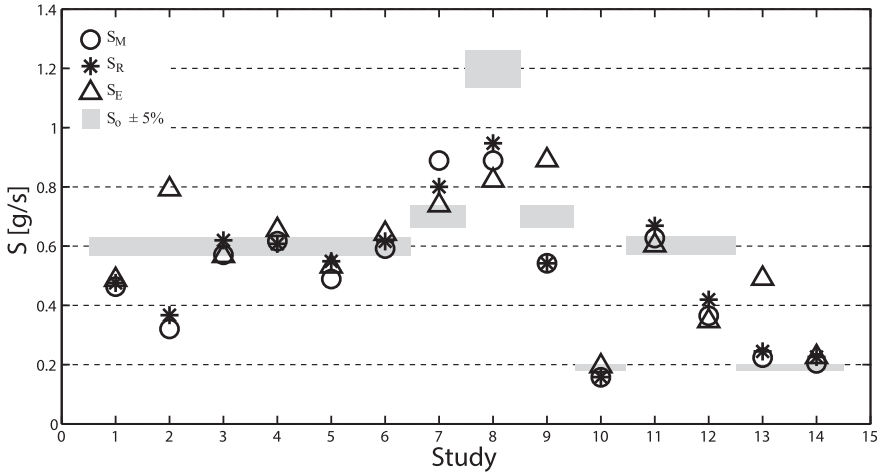


**Fig. 8.** Average source strength ($\overline{S_M}$, $\overline{S_R}$, and $\overline{S_E}$) for each CR study.

topic by presenting two inverse Gaussian source emision rate estimation schemes based on modeled and a reconstructed plumes.

The results of this study show that three different treatments of plume geometry and emission calculations have approximately the same source estimate error (Fig. 7) with similar bias levels. This suggests that errors associated with the methods are likely due in part to method assumptions such as the ability of the observation to obtain an ensemble concentration representative of the source emission. The Wyoming results show $S_M$ and $S_R$ are consistently greater than $S_E$. More field studies are necessary to understand the meteorological conditions related to this difference. The CR results suggest multiple observations can help reduce error in source strength assessment using this type of near-field inverse scheme when three or more observations are conducted at each study. These factors should be the subject of further study for OTM 33A and other mobile and fenceline inspection approaches. The methods described in this paper are for the baseline case with assumed continuous emission rates. Future efforts will incorporate time-dependent variations in emissions that may be related to routine maintenance activities (e.g. liquids unloading).

## Acknowledgments

This work was supported by the NSF IGERT through Grant # DGE-1068871 and U.S. EPA ORDs Air, Climate, and Energy (ACE) program. The views expressed in this article are those of the authors and do not necessarily represent the views or policies of the U.S. Environmental Protection Agency. Mention of trade names or commercial products does not constitute endorsement or recommendation for use.

## Appendix A. Atmospheric dispersion calculations

The wind components are rotated to streamline coordinates. The rotated components along with the sonic temperature are used to evaluate the atmospheric stability. As a measure of atmospheric stability, the Monin-Obukhov length ($L$) is calculated as shown:

$$L = -\frac{u_*^3 \overline{T}}{\kappa g \overline{w'T'}} \tag{A.1}$$

where $\kappa$ is the von Karman constant (set to 0.41), $g$ is the gravitational acceleration (set to 9.81 m/s$^2$), $\overline{T}$ is the mean air temperature, and $\overline{w'T'}$ is the mean covariance of the vertical wind component and sonic temperature (Nieuwstadt, 1978; Obukhov, 1971). The friction velocity $u_*$ is calculated as:

$$u_* = \sqrt{-\overline{u'w'}} \tag{A.2}$$

where $\overline{u'w'}$ is the mean covariance of the horizontal (x) and vertical wind components (z).

The effective height of the plume $\bar{z}$ is calculated with the following equation:

where $c$ is a coefficient dependent on $s$ (set to 0.6), $z_o$ is the

roughness length, $L_x$ is the longitudinal distance off the center of the plume, $L_{x,\mathrm{eff}}$ is the effective distance to the source [$L_{x,\mathrm{eff}} = L_x\cos(\theta - \theta_p)$], and $x_o$ is an integration constant (Gryning et al., 1987). Before calculating $\bar{z}$, $x_o$ is calculated with Eq. (A.3) by setting $L_x = 0$ and $\bar{z}$ to the source height ($z_s$). Once $x_o$ is calculated, $\bar{z}$ is calculated iteratively with $L_x$ now set as the distance to the source. Constants $p$, $a_1$, $b_1$, and $b_2$ are set to 1.55, 16, 5, and 5, respectively (Gryning et al., 1987).

The function $A$ and $B$ are calculated as:

$$L_{x,,\mathrm{eff}} + x_o = \begin{cases} (\bar{z}/\kappa^2)[\ln(c\bar{z}/z_o) - \Psi(c\bar{z}/L)][1 - pa_1\bar{z}/(4L)]^{-1/2} & \text{for } L<0 \\ (\bar{z}/\kappa^2)[\{\ln(c\bar{z}/z_o) + 2b_2p\bar{z}/(3L)\}\{1 + b_1p\bar{z}/(2L)\} + (b_1/4 - b_2/6)p\bar{z}/L] & \text{for } L>0 \end{cases} \quad (A.3)$$

$$A = s\Gamma(2/s)[\Gamma(1/s)]^2 \quad (A.4)$$

$$B = \Gamma(2/s)\Gamma(1/s) \quad (A.5)$$

where $\Gamma$ is the gamma function. The shape parameter ($s$) is calculated as a function of $L$, $\bar{z}$, and $z_o$:

$$s = \begin{cases} \dfrac{1 - a_1c\bar{z}/(2L)}{1 - a_1c\bar{z}/L} + \dfrac{(1 - a_2c\bar{z}/L)^{-1/4}}{\ln(c\bar{z}/z_o) - \Psi(c\bar{z}/L)} & \text{for } L<0 \\ \dfrac{1 + 2b_1c\bar{z}/L}{1 + b_1c\bar{z}/L} + \dfrac{1 + b_2c\bar{z}/L}{\ln(c\bar{z}/z_o) + \Psi(\bar{z}/L)} & \text{for } L>0 \end{cases} \quad (A.6)$$

where $\Psi$ is a stability parameter dependent on $\bar{z}$ and $L$ (Gryning et al., 1987).

For a given elevation, the $\Psi$ is calculated as:

$$\Psi\left(\frac{z}{L}\right) = \begin{cases} (1 - a_2z/L)^{1/4} - 1 & \text{for } L<0 \\ -b_2z/L & \text{for } L>0 \end{cases} \quad (A.7)$$

where $a_2 = 16$ and $b_2 = 5$ (Gryning et al., 1983, 1987; Eckman, 1994; Dyer, 1974).

In this study, $z_o$ is calculated with the following equation:

$$U(z) = \frac{u_*}{\kappa}\left[\ln\left(\frac{z}{z_o}\right) - \Psi\left(\frac{z}{L}\right)\right] \quad (A.8)$$

where $z$ is $z_m$ and $U(z)$ is the measured mean velocity at the measurement height, $z$ (Eckman, 1994). The mean transport velocity $\overline{U}$ is calculated at the mean plume height $z = \bar{z}$ where $z = c\bar{z}$ for $L<0$ and $z = \bar{z}$ for $L>0$.

## References


Allen, D.T., Pacsi, A.P., Sullivan, D.W., Zavala-Araiza, D., Harrison, M., Keen, K., Fraser, M.P., Daniel Hill, A., Sawyer, R.F., Seinfeld, J.H., 2014. Methane emissions from process equipment at natural gas production sites in the united states: pneumatic controllers. Environ. Sci. Technol. 49 (1), 633–640.

Allen, D.T., Torres, V.M., Thomas, J., Sullivan, D.W., Harrison, M., Hendler, A., Herndon, S.C., Kolb, C.E., Fraser, M.P., Hill, A.D., et al., 2013. Measurements of methane emissions at natural gas production sites in the united states. Proc. Natl. Acad. Sci. 110, 17768–17773.

Brandt, A., Heath, G., Kort, E., OSullivan, F., Pétron, G., Jordaan, S., Tans, P., Wilcox, J., Gopstein, A., Arent, D., et al., 2014. Methane leaks from north american natural gas systems. Science 343, 733–735.

Brantley, H.L., Thoma, E.D., Eisele, A.P., 2015. Assessment of VOC and HAP Air Emissions from Oil and Natural Gas Well Pads Using Mobile Remote and Onsite Direct Measurements. J. Air Waste Manag. (submitted for publication).

Brantley, H.L., Thoma, E.D., Squier, W.C., Guven, B.B., Lyon, D., 2014. Assessment of methane emissions from oil and gas production pads using mobile measurements. Environ. Sci. Technol. 48, 14508–14515.

Carbon Limits (CL), 2013. Quantifying Cost-effectiveness of Systematic Leak Detection and Repair Programs Using Infrared Cameras. URL: http://catf.us/resources/publications/view/198.

DOE ARPA-E, 2014. Methane Observatin Networks with Innovative Technology to Obtain Resductions – MONITOR. URL: http://arpa-e.energy.gov/sites/default/files/documents/files/MONITOR%20and%20DELTA%20Project%20Descriptions_Final_12.15.14.pdf.

Dyer, A., 1974. A review of flux-profile relationships. Boundary 363–372.

Eckman, R., 1994. Re-examination of empirically derived formulas for horizontal diffusion from surface sources. Atmos. Environ. 28, 265–272.

EDF, 2015. Methane Detectors Challenge. URL: http://www.edf.org/energy/natural-gas-policy/methane-detectors-challenge.

ERG, 2011. City of Fort Worth Natural Gas Air Quality Study, Final Report. Prepared for the City of Fort Worth, Texas. URL: http://fortworthtexas.gov/gaswells/default.aspx?id=87074.

Gifford, F., 1959. Statistical properties of a fluctuating plume dispersion model. Adv. Geophys. 6, 117–137.

Gryning, S., Holtslag, A., Irwin, J., Sivertsen, B., 1987. Applied dispersion modelling based on meteorological scaling parameters. Atmos. Environ. (1967) 21, 79–89.

Gryning, S., Van Ulden, P., Larsen, R., 1983. Dispersion from a continuous ground level source investigated by a k model. Q. J. R. Meteorological Soc. 109, 355–364.

Horst, T., Weil, J., 1992. Footprint estimation for scalar flux measurements in the atmospheric surface layer. Boundary-Layer Meteorol. 59, 279–296.

Howard, T., Ferrara, T., Townsend-Small, A., 2015. Sensor transition failure in the high flow sampler: Implications for methane emission inventories of natural gas infrastructure. J. Air & Waste Manag. Assoc. http://dx.doi.org/10.1080/10962247.2015.1025925.

Lamb, B.K., Edburg, S.L., Ferrara, T.W., Howard, T., Harrison, M.R., Kolb, C.E., Townsend-Small, A., Dyck, W., Possolo, A., Whetstone, J.R., 2015. Direct measurements show decreasing methane emissions from natural gas local distribution systems in the United States. Environ. Sci. Technol. URL: http://pubs.acs.org/doi/full/10.1021/es505116p.

Monin, A., Obukhov, A., 1954. Basic laws of turbulent mixing in the surface layer of the atmosphere. Contrib. Geophys. Inst. Acad. Sci. USSR 151, 163–187.

Nieuwstadt, F., 1978. The computation of the friction velocity u* and the temperature scale t* from temperature and wind velocity profiles by least-square methods. Boundary-Layer Meteorol. 14, 235–246.

Obukhov, A., 1971. Turbulence in an atmosphere with a non-uniform temperature. Boundary-Layer Meteorol. 2, 7–29.

Pasquill, F., Smith, F., 1983. Atmospheric Diffusion, third ed. Ellis Horwood Limited.

Rella, C.W., Tsai, T.R., Botkin, C.G., Crosson, E.R., Steele, D., 2015. Measuring emissions from oil and natural gas well pads using the mobile flux plane technique. Environ. Sci. Technol. 49 (7), 4742–4748.

Sutton, O., 1953. Micrometeorology: A Study of Physical Processes in the Lowest Llayer of the Earth's Atmosphere. McGraw-Hill Book Company, New York.

Turner, D.B., 1994. Workbook of Atmospheric Dispersion Estimates: An Introduction to Dispersion Modeling/Book and Disk. CRC Press.

van Ulden, A., 1978. Simple estimates for vertical diffusion from sources near the ground. Atmos. Environ. (1967) 12, 2125–2129.

U.S. EIA, 2012a. Total Energy Annual Energy Review. Table 5.2 Crude Oil Production and Crude Oil Well Productivity, Selected Years, 1954-2011. URL: http://www.eia.gov/total energy/data/annual/pdf/sec5_9.pdf.

U.S. EIA, 2012b. Total Energy Annual Energy Review. Table 6.4 Natural Gas Gross Withdrawals and Natural Gas Well Productivity, Selected Years, 1960-2011. URL: http://www.eia.gov/total energy/data/annual/pdf/sec6_11.pdf.

U.S. EIA, 2013. Drilling Often Results in Both Oil and Natural Gas Production. URL: http://www.eia.gov/todayinenergy/detail.cfm?id=13571.

U.S. EPA, 1995. Protocol for Equipment Leak Emission Estimates. Office of Air Quality Planning and Standards. URL: http://www.epa.gov/ttnchie1/efdocs/equiplks.pdf.

U.S. EPA, 2010. Greenhouse Gas Emissions Reporting from the Petroleum and Natural Gas Industry, Background Technical Supporting Document, Supporting 40 Cfr Part 98.230. 77 Fr 11039 Subpart W- Petroleum and Natural Gas Systems. URL: http://www.epa.gov/ghgreporting/documents/pdf/2010/Subpart-W_TSD.pdf.

U.S. EPA, 2014a. Oil and Natural Gas Sector Leaks, Report for Oil and Natural Gas Sector Leaks Review Panel. URL: http://www.epa.gov/airquality/oilandgas/2014papers/20140415leaks.pdf.

U.S. EPA, 2014b. Other Test Method (OTM) 33 and 33A Geospatial Measurement of Air Pollution-remote Emissions Quantification-direct Assessment (GMAP-reqda). URL: http://www.epa.gov/ttn/emc/prelim/otm33a.pdf.